applied sciences

MDPI

Article

Exponentially Graded Auxetic Structures: An Assessment of the Shear Correction Factor and Static Deflection

Maria Amélia R. Loja [1,2,*] and Joaquim I. Barbosa [1,2]

[1] CIMOSM—Centro de Investigação em Modelação e Otimização de Sistemas Multifuncionais, ISEL/IPL—Instituto Superior de Engenharia de Lisboa, Av. Conselheiro Emídio Navarro 1, 1959-007 Lisboa, Portugal; joaquim.barbosa@isel.pt

[2] IDMEC—IST-Instituto Superior Técnico, Universidade de Lisboa, Av. Rovisco Pais 1, 1049-001 Lisboa, Portugal

* Correspondence: amelia.loja@isel.pt

Abstract: This work aims to study the influence of the material and geometric parameters that characterize re-entrant hexagonal honeycomb auxetic structures in the maximum transverse static deflection of beams. In addition, this study considers the composition of the material through the thickness results from the mixture of a metallic phase and one of four different selected ceramics, using the exponential volume fraction law. The first-order shear deformation theory within an equivalent single-layer approach is used to assess the material and geometric parameters' influence on the structures' deflection. Considering this theoretical approach, the impact of the material and geometric parameters on the shear correction factors, calculated for each specific case, is also analyzed. The results allow us to conclude how the shear correction factors and the structures' maximum static deflection are affected by the re-entrant hexagonal honeycomb auxetic cells' aspect ratios, by the angle associated with the direction of the inclined members of the hexagonal cells and the use of materials with differentiated Poisson's ratios.

Keywords: re-entrant hexagonal honeycomb structures; auxetic materials; exponentially graded materials; first-order shear deformation theory; shear correction factor; finite-element analysis

Citation: Loja, M.A.R.; Barbosa, J.I. Exponentially Graded Auxetic Structures: An Assessment of the Shear Correction Factor and Static Deflection. *Appl. Sci.* **2024**, *14*, 9356. https://doi.org/10.3390/app14209356

Academic Editor: Victor Franco Correia

Received: 13 September 2024
Revised: 8 October 2024
Accepted: 11 October 2024
Published: 14 October 2024

1. Introduction

Honeycomb structures, nature-inspired by bee honeycombs, can be found in a diversity of fields, such as engineering, architecture, and biomedicine, and are a topic of interest both in terms of their structural analysis and their optimal design, as the research literature can show. Extending this structural configuration to auxeticity characteristics, namely by considering negative Poisson's ratio materials, it is possible to obtain materials and structures that are able to exhibit high specific strength, stiffness, superior energy absorption, and indentation resistance, making them highly valuable in industries, like aerospace, medicine, defense, and sports, among others.

As far as it is possible to understand from the published works, and without aiming to establish an exhaustive historical line, it is important to refer to some key works in this context. The term auxetic was introduced into the scientific literature by Evans (1991) [1], who emphasized the importance of the Poisson ratio to material performance improvement. However, some published works on structures with negative Poisson's ratio materials were already published. It is the case of the work of Almgren (1985) [2], where mechanical structures with a Poisson's ratio equal to minus one were proposed. It is also the case of the method first proposed by Lakes (1987) [3] to create the reentrant structure of an auxetic foam, which proved to be more resilient than conventional foams. Wojciechowski (1989) [4] pioneered the computational study of isotropic two-dimensional chiral molecular models, considering the spontaneous formation of auxetic phases. In this sequence, a family of two-dimensional, biphasic composite materials with hexagonal symmetry was

studied by Milton (1992) [5], who showed that two- and three-dimensional composites with a Poisson's ratio approaching the value −1 could be obtained through a selective design with specific layups involving separated length scales. Later, Baughman et al. (1998) demonstrated experimentally that negative Poisson ratios were common on cubic metals, a useful feature to reverse the compensation effect of positive Poisson ratios on the volume and area changes caused by uniaxial stress.

In more recent years, it has been possible to find several published works where the design, development, properties characterization, and performance analysis of these material structures are often found, mainly in the context of sandwich configurations. However, only a few published studies consider that these material structures can be hybridized by graded mixtures of their material constituents [6]. Hence, the literature overview in this introductory section follows a categorization vector, starting with highlighting some of the review works.

A review study on the design, fabrication, and optimization of honeycomb structures, developed by Zhang et al., 2015 [7], focused on the properties related to structure, scale, and materials and highlighted their potential in biomedical applications, like tissue engineering and regenerative medicine. Some years later, another review focused on sandwich structures, emphasizing their light weight, high performance, excellent strength-to-weight ratios, and energy absorption, was presented by Sahu et al. (2022) [8]. These authors considered various core types, face sheet materials, and joining methods. Other review studies in the context of auxetic structured materials were also published in parallel, such as the work of Evans and Alderson (2000) [9], highlighting the significant advancements in auxetic materials, and noting their growing use in functional and structural applications. According to the authors, this field was rapidly evolving with new materials and processing methods, indicating substantial potential for future applications. Prawoto (2012) [10] also did a review focused on auxetic materials, focusing on the computational and mechanical aspects. In that work, in addition to the importance of auxetic materials, a potential shift from ordered microstructures to disordered ones using the homogenization method was pointed out as future work. More recently, Liu et al. (2023) [11] examined the principles of auxeticity, mechanical properties, and applications in medicine, automotive manufacturing, and protective gear, highlighting future development directions for auxetic metamaterials. These authors categorized auxetic honeycomb structures into re-entrant, chiral, and rotational rigid types, comparing their mechanisms and properties.

Different authors addressed the problem of characterizing honeycomb and auxetic materials' properties, adopting experimental and/or numerical/analytical approaches. Masters and Evans (1996) [12] developed a theoretical model to predict the elastic constants of honeycombs by considering deformation mechanisms, hence obtaining expressions for the tensile moduli, shear moduli, and Poisson's ratios. Strek et al. (2015) [13] studied the effective properties and dynamic response of a sandwich panel consisting of two face sheets and an auxetic core with a filler material, having found that auxetic sandwich panels could be created with two solid materials having positive Poisson ratios, showing significant structural and dynamic benefits. Numerical simulations were performed by Scarpa and Tomlin (2000) [14] to determine the transverse shear modulus of honeycombs with in-plane negative Poisson's ratios. The results revealed that the modulus lies between the theoretical upper and lower bounds and varies with the relative density and the gauge-thickness ratio. Gao et al. (2022) [15] proposed an analytical framework to predict the in-plane mechanical properties of auxetic structures. To reduce stress shielding at the bone–implant interface by adjusting the elastic modulus to better match the bone, Mohammadi Ghalehney et al. (2024) [16] recently used experimental and numerical methods to obtain the elastic modulus of gradient structures with auxetic unit cells. Zhang et al. (2024) [17] used the Euler–Bernoulli beam theory to derive the equivalent elastic properties of auxetic cellular structures with irregular configurations. The impact of cell height and inclination angle on the in-plane linear elastic properties was examined. Under quasi-static compressive loading, the results showed that the gradient cell size minimally affects elastic behavior

and energy absorption. Bidirectional gradient structures exhibited higher platform stress, while homogeneous small-size structures exhibited the highest load-bearing and energy-absorption capacities.

In a complementary field, it is also possible to find studies mainly focused on the design and development of auxetic unit cells. This is the case of the work of Valle et al. (2021) [18], who proposed an asymmetric 3D auxetic structure, designed using Timoshenko beam theory and based on a 2D cell configuration. The new design, tested through quasi-static compression tests of ABS samples obtained by fused filament fabrication, was shown to be aligned with the theoretical predictions. Bhullar et al. (2022) [19] developed and characterized a stainless-steel stent with a re-entrant hexagonal cell geometry, micromachined using a high-precision femtosecond laser. The mechanical behaviors under various loadings were analyzed, and the stent demonstrated superior bending, twisting, and buckling resistance, ensuring maintained blood flow. More recently, an architected lattice system inspired by ancient Chinese window grills, combining chiral and re-entrant properties was investigated by Luo et al. (2023) [20]. Experiments and simulations demonstrated a significant negative Poisson's ratio effect, influenced by the structure's geometric parameters.

Another relevant research direction regards mechanical behavior prediction, wherein several published studies on auxetic structures are found. Among others, one refers to the work of Qing-Tian and Zhi-Chun (2010) [21], who derived wave propagation equations in three-layer sandwich panels with auxetic cores, using a semi-analytical finite-element method. Conventional hexagonal and re-entrant auxetic cores were compared, exploring how panel thickness, unit cell geometry, and variations in the Poisson's ratio and core density affect dispersive curves. Shokri Rad et al. (2014) [22] explored the microstructure of auxetic materials by simplifying them into distinct mechanisms, focusing on adapting a 2D re-entrant structure to a 3D auxetic structure due to its similar fundamental characteristics. Chen and Feng (2017) [23] modeled the dynamic response of a supported laminated plate with in-plane excitation by considering von Kármán theory. Duncan et al. (2018) [24] investigated the use of open-cell polyurethane auxetic foams in sports helmets to improve impact acceleration attenuation. The results suggested that using these materials in helmets can better attenuate impact severity, potentially reducing the risk of traumatic brain injuries in sports. The nonlinear dynamic response and vibration of sandwich cylindrical panels, with an auxetic honeycomb core sandwiched between isotropic aluminum skins, were studied by Duc (2017) [25]. The authors used first-order shear deformation theory to examine how geometrical parameters, material properties, and different types of loads affect the panels' performance. Nguyen and Pham (2018) [26] analyzed the nonlinear dynamic response and vibration of sandwich plates with auxetic honeycomb cores under blast and mechanical loads, using first-order shear deformation plate theory and analytical methods. Zhu et al. (2019) [27] investigated the frequencies and energy in a honeycomb sandwich plate with a negative Poisson's ratio using Reddy's third-order shear deformation, von Karman nonlinear theory, and Hamilton theory to derive motion equations. The results showed that, while the trends in frequencies and energy are consistent across methods, natural frequencies and potential energies differ in lateral vibrations. The dynamic response of sandwich composite plates with an auxetic honeycomb core under a moving oscillator load was investigated by Tran et al. (2020) [28]. The authors used Mindlin plate theory and the finite-element method to study how the structural parameters, material properties, and load effects influenced the plate's response. Safikhani et al. (2023) [29] studied the energy absorption and negative Poisson's ratio of a re-entrant auxetic structure under quasi-static compression compared to a non-auxetic honeycomb. The behavior was influenced by unit cell geometry, with a higher negative Poisson's ratio achieved by increasing the oblique length and initial angle, while an increased thickness led to a higher Poisson's ratio and reduced auxetic properties.

As previously mentioned, most honeycomb auxetic structures do not consider the possibility of being built of gradually changing mixtures of different materials as generically happens in a functionally graded material. In this context, and to briefly quote the potential

of such materials, it is relevant to refer to the study developed by Birman and Bird (2007) [30] who reviewed key advancements in functionally graded materials (FGMs) since 2000, covering theories, heat transfer, stress analysis, manufacturing, and applications. This work also identified the critical areas requiring further research to enhance the successful implementation of FGMs in design. From the literature, it was concluded that only a few works combining the auxetic unit cell concept with a smooth variation of material mixtures were found, as is the case of the work by Zhang et al. (2021) [31] who investigated a functionally graded sandwich plate with a honeycomb auxetic core. The authors used Reddy's higher-order shear deformation theory to analyze how various parameters affected frequencies and the plate's dynamic response to low-speed impacts. Li et al. (2022) [32] investigated the free vibration and sound insulation of functionally graded honeycomb sandwich plates with a negative Poisson's ratio using derived dynamic equations validated by finite-element simulations. These authors found that such plates, with a negative Poisson's ratio, provided lower frequencies.

In this context, the present study aims to characterize the influence of geometrical and material parameters in the maximum static deflection of re-entrant hexagonal honeycomb auxetic functionally graded beams using the first-order shear deformation theory (Mindlin (1951) [33], Reissner (1945) [34]) and the finite-element method. Considering that this theory requires a shear correction factor, the influence of such parameters on this coefficient is also addressed. In the present study, it is not intended to account for material and geometrical uncertainty, as in Carvalho et al. (2017) [35] and Rosa et al. (2018) [35,36], for example.

Regarding the innovative character of the present work, different aspects differentiate this work from other published ones.

The objects of this work are re-entrant hexagonal honeycomb auxetic structures without the influence of external layers, typical of sandwich configurations which most published works address.

These honeycomb auxetic structures, structural composite materials by nature, may additionally assume a varying material composition through their thickness. This work considers that this variation is ruled by an exponential volume fraction law, where the constituent materials comprise a set of ceramic materials and one metallic material. In the present work, the composition of the material for each thickness coordinate is, thus, defined by the exponential law volume fraction that involves the constituent materials assumed to exist on the bottom and top surfaces of the structure.

The very few known studies considering functionally graded auxetic materials define the evolution of the materials' mixture through the structure thickness, according to the combination of the power-law volume fraction and the rule of mixtures.

Additionally, considering that the first-order shear deformation theory is used in this work, the shear correction factors are calculated for each case, as the material and geometric parameters will significantly differ on a case-by-case basis. The published studies based on the same theoretical approach do not consider this aspect.

The structure of this article, and in particular the remainder of this work, is organized into three main sections. The next section, the second one, presents the main theoretical aspects, while in the third section, the results obtained either from the verification cases or the case studies, are presented and discussed. Finally, the fourth section is devoted to the conclusions.

2. Materials and Methods

This section presents the main theoretical aspects of the present study framework.

2.1. Exponential Functionally Graded Materials

The following exponential volume fraction function, V_f, (Rosa et al., 2018) [36] describes the materials' continuous mixture that occurs through the structure thickness, h:

$$V_f = e^{(-\delta(1-\frac{2z}{h}))} \quad (1)$$

where the thickness coordinate is represented by z and varies between $-h/2$ and $h/2$. According to this, if the volume fraction in Equation (1) refers to the ceramic ($V_f = V_{fc}$), and the ceramic phase is considered to vary from 0 at the bottom to 1 at the top surface, then a generic property P of the FGM obeying this volume fraction evolution is given as:

$$\begin{aligned} \delta &= \tfrac{1}{2} ln\left(\tfrac{Pc}{Pm}\right) \\ P_{FGM} &= P_c V_{fc} \end{aligned} \tag{2}$$

In the present case, the subscripts c and m stand for the ceramic and metallic materials, respectively. The subscript FGM identifies the resulting composite materials, assuming no porosities exist (Reddy, 2000) [37].

The volume fraction evolution through the thickness is associated with the exponential volume fraction and is depicted in Figure 1 for two functionally graded materials. The first FGM is made of carbon tungsten and aluminum, and the second FGM is made of zirconia and aluminum. For this illustrative purpose, the thickness is unitary. As it is possible to observe, although the volume fraction varies between 0 and 1 as expected, the curve depends on the relation between the magnitudes of the constituent materials property that is to be assessed next for the FGM. In this case, the evolution of Young's modulus would be calculated next, as seen in Figure 2.

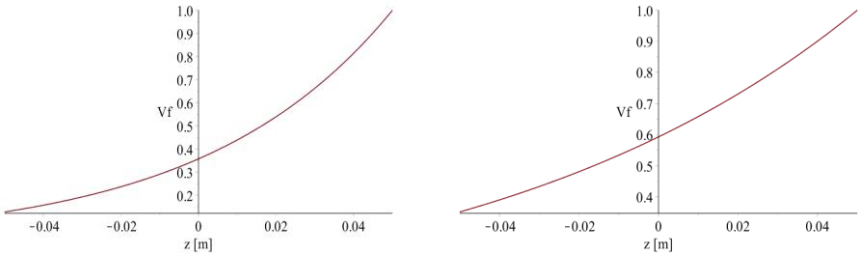

Figure 1. Exponential volume fraction for a unitary thickness FGM beam of (**a**) carbon tungsten–aluminum; (**b**) zirconia–aluminum.

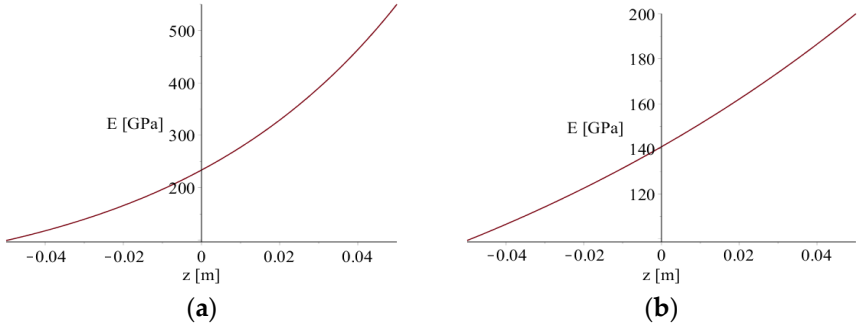

Figure 2. Young modulus through the thickness for a unitary thickness FGM beam of (**a**) carbon tungsten–aluminum; (**b**) zirconia–aluminum.

Figure 2 illustrates the evolution of Young's modulus through the thickness of beams with a unitary thickness made of the previous FGM.

In any case, there is only aluminum at the bottom surface. On the top surface, there is carbon tungsten or zirconia, respectively, for Figure 2a or Figure 2b.

2.2. Re-Entrant Hexagonal Honeycomb Auxetic Materials

The structural material that one aims to consider, in addition to being functionally graded through the thickness, as referred to in the previous sub-section, may also be a re-entrant hexagonal auxetic material, as detailed in [10,11]. Thus, similarly to [31],

who instead considered a power-law volume fraction and rule of mixtures approach, the corresponding equivalent elasticity parameters are here described as:

$$\begin{gathered} E_1 = E_c V_c \frac{\eta 3^3(\eta 1 - sin\theta)}{cos^3(\theta)\left[1+\left(tan^2(\theta)+\eta 1 sec^2(\theta)\right)\eta 3^2\right]} \\ E_2 = E_c V_c \frac{\eta 3^3}{cos(\theta)(\eta 1 - sin(\theta))\left(tan^2(\theta)+\eta 3^2\right)} \\ G_{12} = E_c V_c \frac{\eta 3^3}{\eta 1(1+2\eta 1)cos(\theta)} \\ G_{13} = G_c V_c \frac{\eta 3}{2cos(\theta)}\left[\frac{\eta 1 - sin(\theta)}{1+2\eta 1} + \frac{\eta 1 + 2sin^2(\theta)}{2(\eta 1 - sin(\theta))}\right] \\ G_{23} = G_c V_c \frac{\eta 3 cos(\theta)}{\eta 1 - sin(\theta)} \\ \nu_{12} = -V_c \frac{sin(\theta)\left(1-\eta 3^2\right)(\eta 1 - sin(\theta))}{cos^2(\theta)\left[1+\left(tan^2(\theta)+\eta 1 sec^2(\theta)\right)\eta 3^2\right]} \\ \nu_{21} = -V_c \frac{sin(\theta)\left(1-\eta 3^2\right)}{\left(tan^2(\theta)+\eta 3^2\right)(\eta 1 - sin(\theta))} \end{gathered} \tag{3}$$

The coefficients E_1, E_2, G_{12}, G_{13}, G_{23}, v_{12}, and v_{21} are the elasticity moduli, the shear moduli, and the negative Poisson's ratios. The parameters $\eta 1$ and $\eta 3$ stand, respectively, for the re-entrant hexagonal cell aspect ratios d/l and t/l.

The dimensions d and l are the lengths of the horizontal and inclined segments of the honeycomb unit cell, while t is the segments' thickness, assumed to be constant throughout the cell (Figure 3).

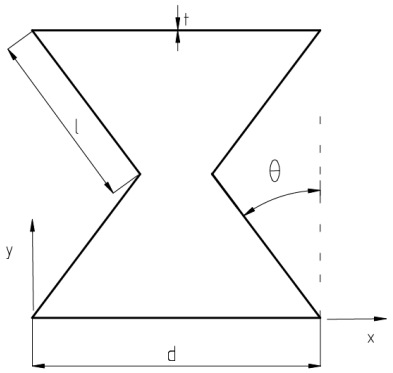

Figure 3. Unit cell of a re-entrant hexagonal honeycomb auxetic material and its relation to the coordinate directions x and y.

According to these definitions, when the angle θ is zero, the cell configuration is generically rectangular. A positive angle variation follows the counterclockwise direction and a negative the clockwise one. In this work, the angle varies discretely within $\{-75°, -60°, -45°, -30°, -15°, 0°, 15°, 30°, 45°, 60°, 75°\}$. The extreme values of the angles considered correspond to the flattening of the unit cell along the x and y directions, respectively.

The relationship between the horizontal and the inclined segments ($\eta 1$) assumes the values in the set {1, 1.25, 1.5, 1.75, 2}.

Concerning the relation between the thickness of the walls' cells and the inclined segment, the ratio ($\eta 3$) can assume the values of the set {0.01, 0.015, 0.02, 0.025, 0.03, 0.035, 0.04, 0.045, 0.05}. The cells' thickness is equal for all the horizontal and inclined segments.

2.3. Shear Deformation Theory and Constitutive Equations

According to the first-order shear deformation theory (FSDT), (Mindlin, 1951) [33], the corresponding displacement field can be written in the following form:

$$\begin{gathered} u(x,y,z) = u^0(x,y) + z.\theta_x^0(x,y) \\ v(x,y,z) = v^0(x,y) + z.\theta_y^0(x,y) \\ w(x,y) = w^0(x,y) \end{gathered} \tag{4}$$

where u, v, and w denote the displacements of a generic point described according to a Cartesian coordinate system of directions (x, y, z). The degrees of freedom are thus $\{u^0, v^0, w^0, \theta_x^0, \theta_y^0\}$ with the superscript o, meaning that the degree of freedom is associated with a point located at the mid-plane surface of the structure. The elastic strains are obtained by considering the kinematical relations for linear elasticity, and the constitutive relation associated with the present theory is written as:

$$\begin{Bmatrix} \sigma_{xx} \\ \sigma_{yy} \\ \sigma_{xy} \end{Bmatrix} = \begin{bmatrix} C_{11} & C_{12} & 0 \\ C_{12} & C_{22} & 0 \\ 0 & 0 & C_{66} \end{bmatrix} \begin{Bmatrix} \varepsilon_{xx} \\ \varepsilon_{yy} \\ \gamma_{xy} \end{Bmatrix}, \begin{Bmatrix} \sigma_{yz} \\ \sigma_{xz} \end{Bmatrix} = \begin{bmatrix} k_{23}.C_{44} & 0 \\ 0 & k_{13}.C_{55} \end{bmatrix} \begin{Bmatrix} \gamma_{yz} \\ \gamma_{xz} \end{Bmatrix} \tag{5}$$

where the stress and strain components are represented as $\{\sigma_{xx} \quad \sigma_{yy} \quad \sigma_{xy}\, \sigma_{yz} \quad \sigma_{xz}\}$ and $\{\varepsilon_{xx} \quad \varepsilon_{yy} \quad \gamma_{xy}\, \gamma_{yz} \quad \gamma_{xz}\}$, respectively. The elastic stiffness coefficients C_{ij} are given in the literature (Reddy, 2003) [38]. The coefficients k_{mn} stand for the shear correction factors required when using FSDT (Whitney, 1973) [39]. Although shear correction factors are often considered to be equal to 5/6, in the present work, these factors are determined for each specific case considered (as, for example, in (Mota et al., 2020) [40] and (Mota and Loja), 2023, [41]). In the present study, the approach of (Vlachoutsis, 1992) [42] was considered, where the calculation of the k_{13} coefficient, for example, yields the following expression:

$$k_{13} = \frac{\left[\int_{-h/2}^{h/2} C_{11}(z)(z - z_{n1})^2 dz\right]^2}{\int_{-h/2}^{h/2} G_{13}(z)dz \int_{-h/2}^{h/2} \left(\frac{\left(-\int_{-h/2}^{z} C_{11}(z)(z-z_{n1})dz\right)^2}{G_{13}(z)}\right)dz} \tag{6}$$

where z_{n1} is the thickness coordinate of the neutral surface, taking as reference the mid-surface (z = 0) of the structure.

2.4. Equilibrium Equations

Considering the aim of performing linear elastic static analyses to characterize the static response for the present auxetic exponentially graded plate/structures, one considers the minimum potential energy principle (Zienkiewicz, 2014) [38,43] applied to the entire domain of the structure when submitted only to surface-distributed transverse loads. After integrating into the thickness, one yields:

$$\begin{gathered} \delta(U + W) = 0 \\ \delta U = \int_\Omega \left\{ N_{xx}\delta\varepsilon_{xx} + M_{xx}\delta\kappa_{xx} + N_{yy}\delta\varepsilon_{yy} + M_{yy}\delta\kappa_{yy} + N_{xy}\delta\gamma_{xy} + M_{xy}\delta\kappa_{xy} + Q_y\delta\gamma_{yz} + Q_x\delta\gamma_{xz} \right\} dxdy \\ \delta W = \int_\Omega p_z \delta w^0 dxdy \end{gathered} \tag{7}$$

where U and W represent the elastic strain energy and external forces work, respectively. Meanwhile, Ω stands for the mid-surface of the plate–beam structure, and $(N_{\alpha\beta} \quad M_{\alpha\beta}) = \int_{-h/2}^{h/2} \sigma_{\alpha\beta}(1 \quad z)\, dz$, $(Q_\alpha) = \int_{-h/2}^{h/2} \sigma_{\alpha\beta}\, dz$. The subscripts α, β stand for x, y, and $N_{\alpha\beta}$, $M_{\alpha\beta}$, and Q_α represent the surface internal force, moment, and shear force per unit length. After some manipulation, one yields the equilibrium equations:

$$\begin{gathered} \frac{\partial N_{xx}}{\partial x} + \frac{\partial N_{xy}}{\partial y} = 0\,;\ \frac{\partial N_{xy}}{\partial x} + \frac{\partial N_{yy}}{\partial y} = 0\,;\ \frac{\partial Q_x}{\partial x} + \frac{\partial Q_y}{\partial y} = 0 \\ \frac{\partial M_{xx}}{\partial x} + \frac{\partial M_{xy}}{\partial y} - Q_x = 0\,;\ \frac{\partial M_{xy}}{\partial x} + \frac{\partial M_{yy}}{\partial y} - Q_y = 0 \end{gathered} \tag{8}$$

where the relations between internal generalized forces and strains and the elastic stiffness matrix coefficients of the functionally graded honeycomb auxetic structure are given as:

$$\begin{Bmatrix} N_{xx} \\ N_{yy} \\ N_{xy} \end{Bmatrix} = \begin{bmatrix} A_{11} & A_{12} & 0 \\ A_{12} & A_{22} & 0 \\ 0 & 0 & A_{66} \end{bmatrix} \begin{Bmatrix} \varepsilon_{xx} \\ \varepsilon_{yy} \\ \gamma_{xy} \end{Bmatrix}, \begin{Bmatrix} M_{xx} \\ M_{yy} \\ M_{xy} \end{Bmatrix} = \begin{bmatrix} D_{11} & D_{12} & 0 \\ D_{12} & D_{22} & 0 \\ 0 & 0 & D_{66} \end{bmatrix} \begin{Bmatrix} \kappa_{xx} \\ \kappa_{yy} \\ \kappa_{xy} \end{Bmatrix} \quad (9)$$
$$\begin{Bmatrix} Q_x \\ Q_y \end{Bmatrix} = \begin{bmatrix} k_{23}\hat{A}_{44} & 0 \\ 0 & k_{13}\hat{A}_{55} \end{bmatrix} \begin{Bmatrix} \gamma_{yz} \\ \gamma_{xz} \end{Bmatrix}$$

$$\begin{aligned} (A_{ij} \quad D_{ij}) &= \int_{-h/2}^{h/2} C_{ij}(1 \quad z^2)dz, \qquad i,j = 1,2,6 \\ (\hat{A}_{ij}) &= \int_{-h/2}^{h/2} C_{ij}dz, \qquad i,j = 4,5 \end{aligned} \quad (10)$$

These equilibrium equations were implemented using the finite-element method considering a four-node Lagrange quadrilateral finite element with five degrees of freedom per node. A selective integration method was considered for the transverse shear contribution (Zienkiewicz, 2014; Ramos Loja et al., 1997) [43,44].

3. Results and Discussion

Before considering the case studies where the influence of geometrical and material parameters of the re-entrant hexagonal honeycomb auxetic material are assessed, the implemented model was compared against two verification cases.

3.1. Verification Cases

3.1.1. Case 1—Maximum Transverse Deflection of Plates

The first verification study considers an isotropic and homogeneous square simply supported plate submitted to a uniform transversely distributed load p_z. A set of edge-to-thickness ratios, (a/h), was considered, and the analyses were performed considering double-symmetry with a 4 × 4 mesh. The results are presented in the non-dimensional form, $\overline{w} = \frac{Eh^3 w}{p_z a^4}$, in Table 1 for a set of edge-to-thickness ratios and compared with the results of other authors. Table 1 also shows the relative deviations between the present model's results and the three reference results. The relative deviations are calculated as $dev(\%) = \left(\overline{w} - \overline{w}_{ref}\right)/\overline{w}_{ref} \times 100$, where $\overline{w}_{ref}$ stands for the reference non-dimensional deflection.

Table 1. Non-dimensional maximum transverse deflection $\overline{w}$ and relative deviations (%).

a/h	Present $\overline{w}$	Sengupta [45] $\overline{w}$	Rao et al. [46] $\overline{w}$	Salerno and Goldberg [47] $\overline{w}$
4	0.05899	0.05873	0.05631	0.05656
5	0.05369	0.05356	0.05201	0.05360
10	0.04661	0.04666	0.04627	0.04632
20	0.04484	0.04494	0.04483	0.04486
a/h	**-**	***dev* (%) [45]**	***dev* (%) [46]**	***dev* (%) [47]**
4	-	0.44	4.76	4.30
5	-	0.24	3.23	0.17
10	-	−0.11	0.73	0.63
20	-	−0.22	0.02	−0.04

As can be observed, the results present a very good agreement with the alternative authors, particularly with (Sengupta, 1991) [45], whose model is based on the Mindlin–Reissner theory and was implemented through a triangular plate bending element with thirty-five degrees of freedom. Regarding the agreement with the remaining references, there is also a good agreement, except for the thick beams where a greater deviation is observed, although only below 5%.

3.1.2. Case 2—Shear Correction Factors for Sandwich Structure with Outer Layers Made of Functionally Graded Materials

The second verification study addresses the determination of shear correction factors for a sandwich structure. This sandwich structure has a metallic core, and the outer layers are made of a metal–ceramic functionally graded material. All the materials involved have a Poisson ratio of 0.3. In this case, the FGM is ruled by the known power-law volume fraction, characterized by an exponent that functions as an adjustment parameter of the materials' mixture evolution through the thickness. The results obtained are presented in Table 2.

Table 2. Shear correction factors for sandwich structure as a function of the power-law exponent and the relationship between the ceramic and metallic materials' Young's modulus.

	E_c/E_m					
N	**1**	**2**	**3**	**4**	**5**	**6**
0	0.8333	0.8333	0.8333	0.8333	0.8333	0.8333
0.2	0.8333	0.8137	0.7921	0.7699	0.7478	0.7262
0.4	0.8333	0.7973	0.7589	0.7214	0.686	0.6532
0.6	0.8333	0.7843	0.7338	0.6865	0.6437	0.6051
1	0.8333	0.7654	0.6993	0.6409	0.5902	0.5464
2	0.8333	0.7395	0.6552	0.5855	0.5281	0.4805
4	0.8333	0.7184	0.6215	0.5451	0.4844	0.4355
6	0.8333	0.7094	0.6075	0.5286	0.4670	0.4178

The results obtained in the present study are fully coincident with those obtained by (Nguyen et al., 2008) [48]. In consequence, the relative deviations, calculated as $dev(\%) = \left(k - k_{ref}\right)/k_{ref} \times 100$, where k_{ref} stand for the reference shear correction factor and are null for all the cases in Table 2. Hence, for the sake of simplicity, Table 2 presents only the values obtained for each combination of E_c/E_m and N.

This coincidence is observed for different degrees of dissimilarity of the constituent materials' Young's modulus (E_c/E_m) and different mixtures' evolution, as denoted by the set of power-law exponents (N) considered.

3.2. Case Studies

The case studies presented in this sub-section intend to characterize the influence of each geometric and material parameter of the re-entrant hexagonal auxetic structure on the shear correction factor and the maximum static deflection of simply supported beams. As mentioned in the introductory section, the beams are only constituted by the honeycomb auxetic structure, with no outer layers typical of a sandwich configuration. This is because it is only the auxetic structure that one aims to study without the typical reinforcement effect of the sandwich configuration's outer layers.

The beam length is the same for all the case studies, and its cross-section is square. In all of the case studies, the beam boundary conditions and the applied transverse loading are the same and correspond to Figure 4.

The materials used and the relevant properties for this work are presented in Table 3.

For simplification purposes, the materials will be mentioned in the text by the designation presented in the second column of Table 3.

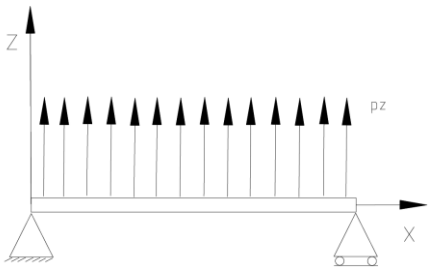

Figure 4. Schematic representation of a simply supported beam submitted to a uniformly distributed transverse loading.

Table 3. Materials' properties.

Material	Designation	E [GPa]	ν
Tungsten Carbide (WC)	WC	550	0.31
Silicon Carbide (SiC)	SiC	440	0.17
Aluminum Oxide (Al_2O_3)	Al_2O_3	370	0.26
Zirconia (ZrO_2)	ZrO_2	200	0.31
Aluminum (Al)	Al	70.3	0.3

3.2.1. Characterization of Poisson's Ratios and Stiffness Coefficients of Re-Entrant Hexagonal Honeycomb Auxetic FGM Beams

With this first case, it is shown how the present auxetic material's Poisson ratios and bending stiffness coefficients vary considering as design parameters, the angle θ, and the unit cell ratio between the length of the horizontal and the inclined segments $\left(\eta 1 = \frac{d}{l}\right)$. To illustrate these profiles, it was assumed that, in this case, the honeycomb auxetic beam has a unit length (a = 1 m) and an aspect ratio a/h = 10. The relation between the unit cell thickness and the inclined segment is $\eta 3 = 0.01$. The functionally graded materials selected are the Al-WC and Al-SiC.

The evolution profiles of the Poisson's ratios for these auxetic FGM can be observed in Figure 5 for the v_{12} at the layer's lower and upper surface. As one observes from Figure 5a), where the constituent materials have close values of Poisson's ratios, the evolution of the Poisson's ratio v_{12} for the range of angles analyzed is very similar, whether one is considering the values assumed at the bottom (inf) or top (sup) surfaces of the beam. However, for the other FGM auxetic beam, where the constituent materials have very different values of Poisson's ratios, the evolution profile of v_{12} differs depending on the thickness coordinate considered. Overall, it is possible to observe that higher absolute values of v_{12} are achieved when the angle θ assumes the values of $-75°$ and $75°$, which correspond to more compact configurations of the re-entrant cells, as these angles characterize more flattened cells. Regarding the effect of the cell aspect ratio η1, it shows a direct influence on v_{12}, i.e., when the relation between the cell horizontal segment and the inclined one increases, this Poisson's ratio also increases. It is also depicted in the figures that the values assumed are slightly higher (in absolute value) when referred to the upper surface in the Al-WC auxetic material in opposition to the Al-SiC one, which shows significantly lower values in the upper surface of the composite (Figure 5b).

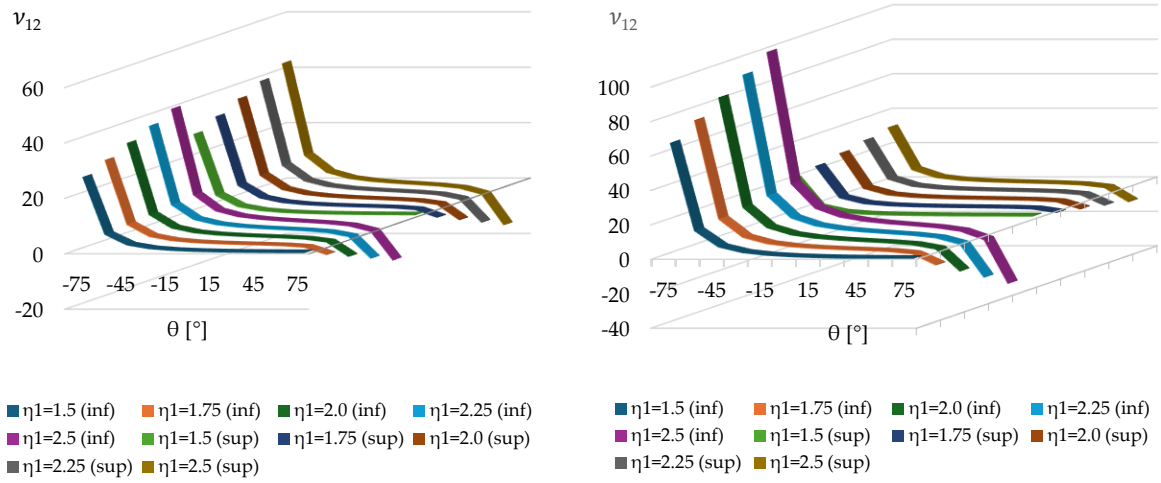

(**a**) (**b**)

Figure 5. Poisson's ratio v_{12} function of angle θ [°] and η1, for η3 = 0.01, (**a**) Al-WC, (**b**) Al-SiC.

If one looks now at Poisson's ratio v_{21} for the same two FGM, the results are observed in Figure 6, again for the bottom and top surfaces of the beam.

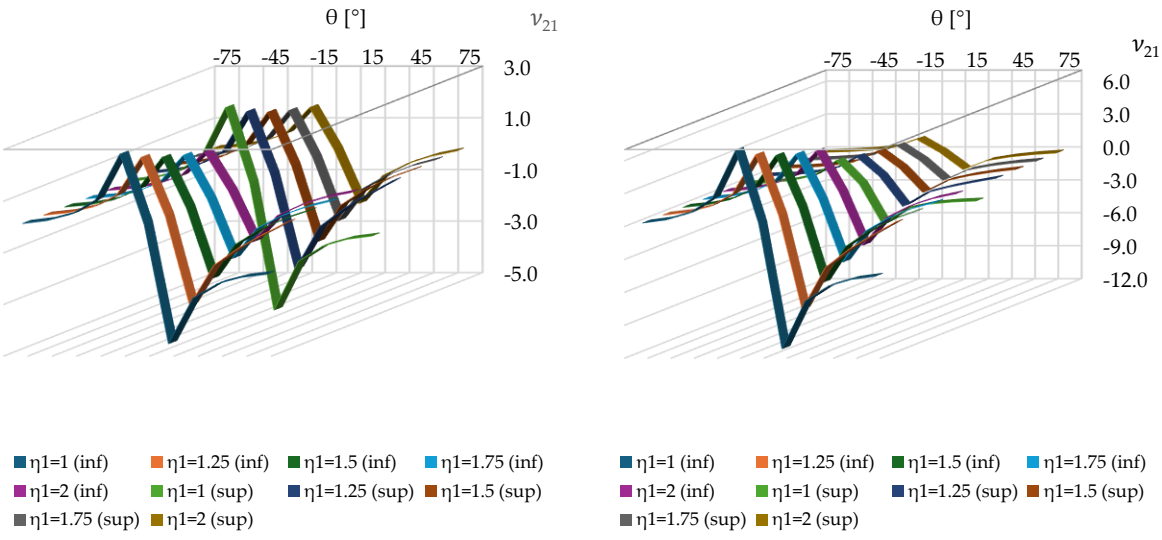

(**a**) (**b**)

Figure 6. Poisson's ratio v_{21} function of angle θ [°] and η1, for η3 = 0.01. (**a**) Al-WC. (**b**) Al-SiC.

As previously, now Figure 6a shows that, in the case of the Al-WC auxetic material, the values assumed for each specific value of η1 at the outer surfaces of the beam are not very different. However, for the Al-SiC auxetic material, the differences between the values observed on the bottom and top surfaces are again greater. In opposition to the effect produced by the ratio η1, in the Poisson's ratio v_{12}, in this case, when η1 increases, it produces a decreasing effect in v_{21}.

In Tables 4 and 5, Poisson's ratios v_{21} for the Al-WC and Al-SiC auxetic material, with η3 = 0.01, are presented for illustrative purposes.

Table 4. Poisson's ratios v_{21} for Al-WC, for η3 = 0.01.

	η1									
	Bottom Surface					**Top Surface**				
θ [°]	**1**	**1.25**	**1.5**	**1.75**	**2**	**1**	**1.25**	**1.5**	**1.75**	**2**
−75	0.0336	0.0298	0.0268	0.0243	0.0223	0.0359	0.0318	0.0286	0.0260	0.0238
−60	0.1473	0.1299	0.1161	0.1050	0.0959	0.1572	0.1387	0.1240	0.1122	0.1024
−45	0.3943	0.3439	0.3049	0.2739	0.2486	0.4210	0.3672	0.3256	0.2925	0.2655
−30	0.9516	0.8157	0.7137	0.6344	0.5710	1.0161	0.8710	0.7621	0.6774	0.6097
−15	2.7222	2.2711	1.9483	1.7059	1.5171	2.9067	2.4251	2.0804	1.8215	1.6199
0	0.0000	0.0000	0.0000	0.0000	0.0000	0.0000	0.0000	0.0000	0.0000	0.0000
15	−4.6234	−3.4572	−2.7609	−2.2980	−1.9681	−4.9367	−3.6916	−2.9480	−2.4538	−2.1015
30	−2.8549	−1.9032	−1.4274	−1.1419	−0.9516	−3.0484	−2.0322	−1.5242	−1.2193	−1.0161
45	−2.2979	−1.2397	−0.8488	−0.6454	−0.5206	−2.4536	−1.3237	−0.9064	−0.6891	−0.5558
60	−2.0510	−0.7156	−0.4334	−0.3109	−0.2423	−2.1900	−0.7641	−0.4628	−0.3319	−0.2587
75	−1.9374	−0.2324	−0.1236	−0.0842	−0.0638	−2.0687	−0.2481	−0.1320	−0.0899	−0.0682

Table 5. Poisson's ratio v_{21} for Al-SiC, for η3 = 0.01.

	η1									
	Bottom Surface					**Top Surface**				
θ [°]	**1**	**1.25**	**1.5**	**1.75**	**2**	**1**	**1.25**	**1.5**	**1.75**	**2**
−75	0.083	0.073	0.066	0.060	0.055	0.027	0.024	0.021	0.019	0.018
−60	0.363	0.320	0.286	0.259	0.236	0.116	0.103	0.092	0.083	0.076
−45	0.971	0.847	0.751	0.675	0.612	0.312	0.272	0.241	0.217	0.197
−30	2.343	2.009	1.758	1.562	1.406	0.752	0.645	0.564	0.502	0.451
−15	6.703	5.593	4.798	4.201	3.736	2.153	1.796	1.541	1.349	1.200
0	0.000	0.000	0.000	0.000	0.000	0.000	0.000	0.000	0.000	0.000
15	−11.385	−8.513	−6.799	−5.659	−4.846	−3.656	−2.734	−2.183	−1.817	−1.556
30	−7.030	−4.687	−3.515	−2.812	−2.343	−2.257	−1.505	−1.129	−0.903	−0.752
45	−5.658	−3.053	−2.090	−1.589	−1.282	−1.817	−0.980	−0.671	−0.510	−0.412
60	−5.051	−1.762	−1.067	−0.765	−0.597	−1.622	−0.566	−0.343	−0.246	−0.192
75	−4.771	−0.572	−0.304	−0.207	−0.157	−1.532	−0.184	−0.098	−0.067	−0.050

Considering the nature of the loadings that will be considered in the present work, namely transverse loadings, it is worth illustrating the bending stiffness coefficients and the transverse shear coefficients associated with the first-order shear deformation theory (without considering the shear correction factor). Figures 7–10 depict those evolutions for illustrative purposes, considering that the relation between the thickness and the length of the unit cell horizontal segment (η3) remains constant and equal to 0.01.

The stiffness coefficient D_{11} for the selected FGM auxetic materials presents different profiles, as depicted in Figure 7. However, it is possible to see that the higher absolute values are obtained for −75°. In both cases, when the ratio between the horizontal and the inclined segments of the cell, $\eta 1$, increases, this bending stiffness also increases (in absolute value).

Opposite trend profiles are visible for the bending stiffness coefficient D_{12} (Figure 8), for the Al-WC, and for the Al-SiC FGM auxetic materials. As in the previous coefficient, this trend is related to the Poisson ratio magnitudes of the constituent materials (the metal and the ceramic) involved in the two materials illustrated.

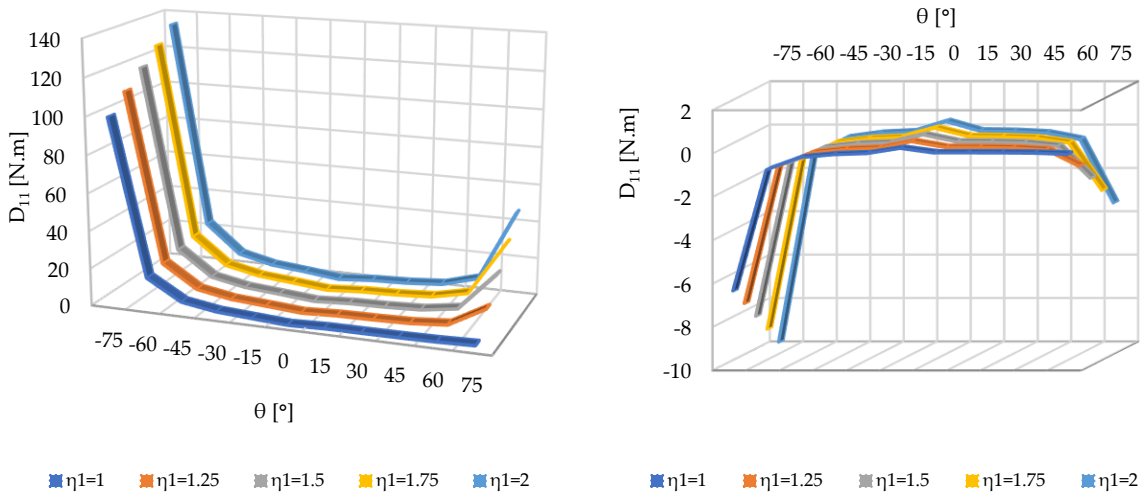

(**a**) (**b**)

Figure 7. Bending stiffness D_{11} [N.m] (**a**) Al-WC, (**b**) Al-SiC.

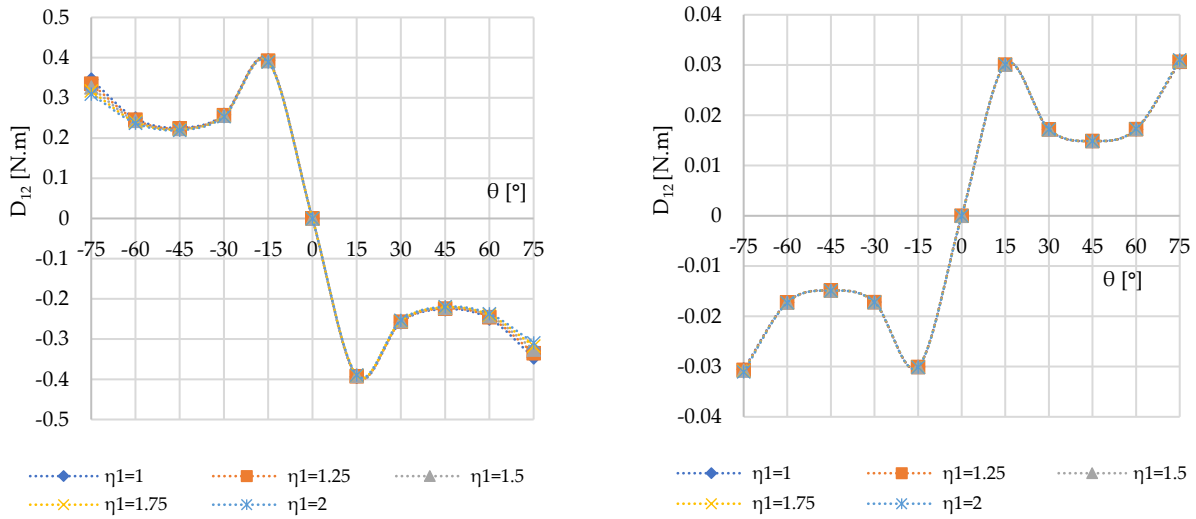

(**a**) (**b**)

Figure 8. Bending stiffness D_{12} [N.m] (**a**) Al-WC, (**b**) Al-SiC.

Figure 9 presents the evolution of the D_{22} coefficient for the sets of angles and $\eta 1$ values considered, being similar for both of the functionally graded auxetic materials, although the higher values assumed occur for the Al-WC material as those that occurred for D_{11}. However, in the present case, these higher values appear for the angle 0°. The increase in $\eta 1$ produces a significant decreasing effect in D_{22}.

To illustrate more briefly the effect of these parameters on the transverse shear stiffness coefficients, Figure 10 depicts the Al-WC auxetic material and the trends observed in the same discrete domains of θ and $\eta 1$. When $\eta 1$ increases, both transverse shear stiffnesses decrease. For A_{55}, the values assumed for the different $\eta 1$ are very close when the angle is between $-75°$ and 45°. However, for higher angle values, the A_{55} decrease is very visible when this ratio increases. Concerning the other stiffness coefficient, A_{44}, the effect of $\eta 1$ demonstrates a visible effect in a greater range of angles.

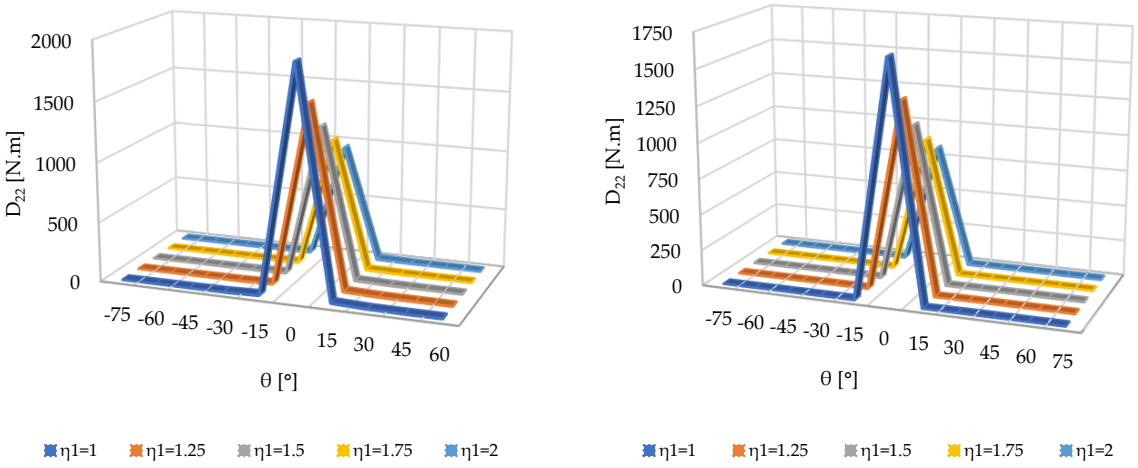

Figure 9. Bending stiffness D22 [N.m] (**a**) Al-WC, (**b**) Al-SiC.

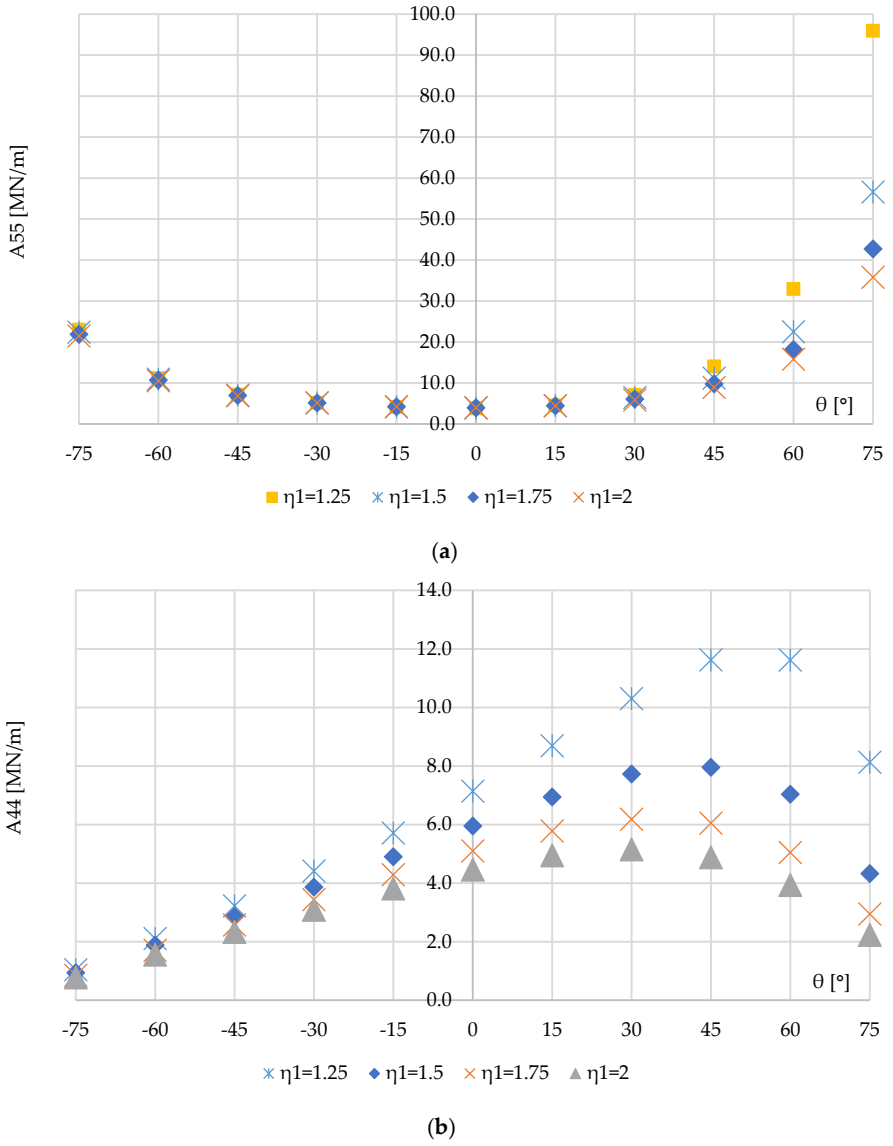

Figure 10. Transverse shear stiffness of Al-WC. (**a**) A_{55}, (**b**) A_{44}.

3.2.2. Influence of Re-Entrant Hexagonal Honeycomb Geometrical Aspect Ratios on the Shear Correction Factor

With this case study, it is intended to investigate the influence of the ratio's $\eta 1$ and $\eta 3$, as well as the angle θ, on the shear correction factors, as determined for each FGM auxetic structure considered in the present work.

To illustrate these influences, one has selected an Al-WC FGM beam with an aspect ratio of a/h = 20. Figures 11 and 12 illustrate the shear correction factors (equal) obtained considering the sets of angles {−75°, −60°, −45°, −30°, −15°, 15°, 30°, 45°, 60°, 75°} and for $\eta 1$ and $\eta 3$: {1, 1.25, 1.5, 1.75, 2} and {0.01, 0.015, 0.02, 0.025, 0.03, 0.035, 0.04, 0.045, 0.05}, respectively. The illustration of the shear correction factor as a function of these parameters is split into two figures to enable an easier visualization. The shear correction factor for the case $\theta = 0°$ assumes a constant value of 0.7692.

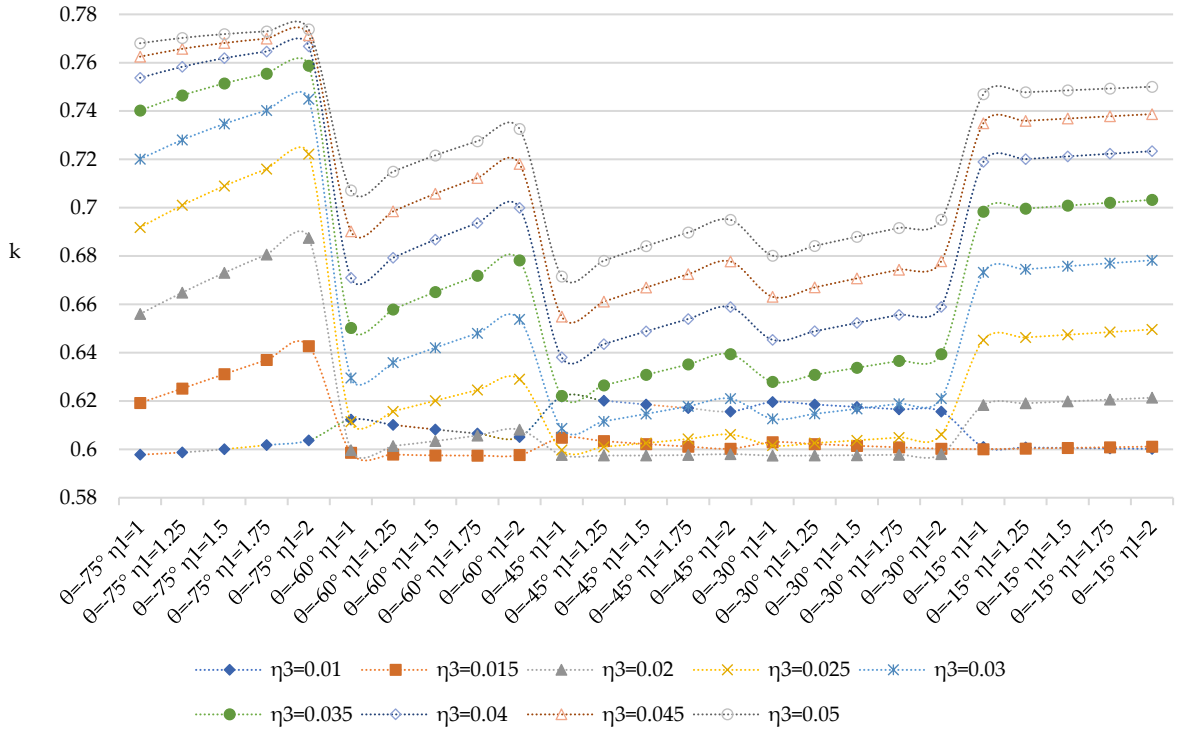

Figure 11. Evolution of shear correction factor as a function of θ, $\eta 1$, and $\eta 3$ for the set of negative angles of the discrete domain.

Overall, from these figures, it is possible to conclude that, when the ratio $\eta 1$ increases, the shear correction factor also increases. For the same angle θ and the same ratio $\eta 3$, these variations are less significant for smaller angle absolute values, e.g., $\theta = -15°$ and $\theta = 15°$, which are very close to the rectangular cell configuration ($\theta = 0°$).

It is also visible that higher values of $\eta 3$ lead to higher values of the shear correction factor, regardless of the angle θ and the ratio $\eta 1$ values. This means that, when the walls of the unit cell are thicker, this translates into a higher shear correction factor.

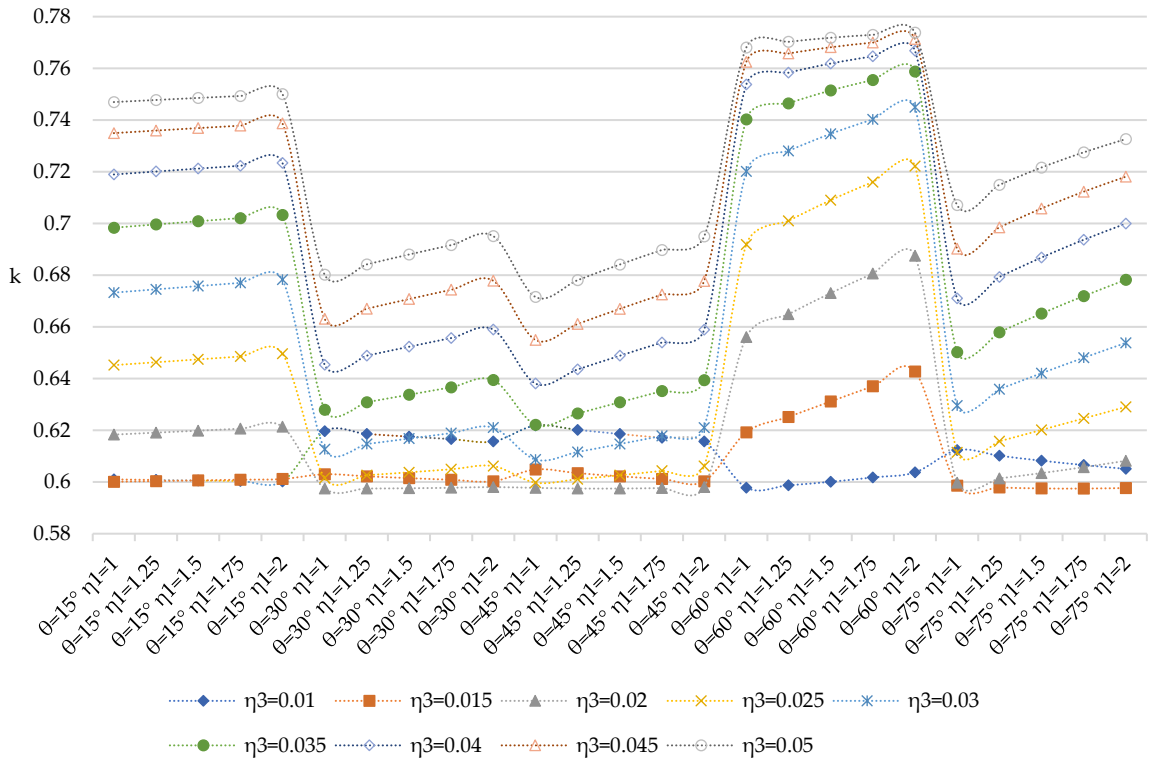

Figure 12. Evolution of shear correction factor as a function of θ, $\eta 1$, and $\eta 3$, for the set of positive angles of the discrete domain.

3.2.3. Influence of Constituent Materials on the Shear Correction Factor

This case aims to study the effect produced using different constituent materials, specifically by considering the different ceramics (Table 3) in the constitution of the honeycomb auxetic FGM, on the shear correction factor value. The beam's length-to-thickness ratio (a/h) is 10. Regarding the unit cell geometric characteristics, one fixed $\eta 3 = 0.01$. The results achieved can be observed in Table 6.

From the results obtained, it can be said that, overall, as the relation between the lengths of the horizontal and inclined segments ($\eta 1$) increases, the value of the shear correction also increases. The exception is the angle $\theta = 0°$, which corresponds to a cell rectangular configuration and where the shear coefficient remains constant for each FGM. For the minor angles (in absolute value), the influence of this ratio is small and, in some cases, is not noticeable for the number of presentation digits.

Regarding the influence of the different ceramic materials and the evolution along the set of angles analyzed, a more restricted presentation is depicted in Figure 13 to provide better legibility.

The curves depicted in Figure 13 represent the evolution of the shear correction factor for the four FGM auxetic cases considered along the set of angles for fixed values of the cells' ratios $\eta 1 = 1$ and $\eta 3 = 0.01$.

From this figure, it is possible to observe that there are two trend profiles. The Al-WC and Al-ZrO_2 FGM auxetic materials show similar evolutions, although with the expected different values. The other trend is shared by the Al-Al_2O_3 and Al-SiC FGM auxetic materials. This is due to the magnitudes of the Poisson's ratios of the different ceramic materials compared to the one of aluminum.

Table 6. Shear correction factor for different FGM auxetic beams with $\eta 3 = 0.01$ as a function of θ and $\eta 1$.

		θ [°]										
Material	**η1**	**−75**	**−60**	**−45**	**−30**	**−15**	**0**	**15**	**30**	**45**	**60**	**75**
Al-WC	1	0.5978	0.6123	0.6219	0.6196	0.6010	0.7692	0.6010	0.6196	0.6219	0.6123	0.5978
	1.25	0.5987	0.6102	0.6202	0.6186	0.6008	0.7692	0.6008	0.6186	0.6202	0.6102	0.5987
	1.5	0.6001	0.6082	0.6186	0.6176	0.6006	0.7692	0.6006	0.6176	0.6186	0.6082	0.6001
	1.75	0.6018	0.6066	0.6171	0.6166	0.6004	0.7692	0.6004	0.6166	0.6171	0.6066	0.6018
	2	0.6037	0.6051	0.6157	0.6157	0.6002	0.7692	0.6002	0.6157	0.6157	0.6051	0.6037
Al-SiC	1	0.6736	0.6621	0.6605	0.6608	0.6659	0.7698	0.6659	0.6608	0.6605	0.6621	0.6736
	1.25	0.6759	0.6625	0.6607	0.6609	0.6661	0.7698	0.6661	0.6609	0.6607	0.6625	0.6759
	1.5	0.6783	0.6630	0.6609	0.6611	0.6662	0.7698	0.6662	0.6611	0.6609	0.6630	0.6783
	1.75	0.6807	0.6635	0.6612	0.6613	0.6663	0.7698	0.6663	0.6613	0.6612	0.6635	0.6807
	2	0.6833	0.6640	0.6614	0.6614	0.6665	0.7698	0.6665	0.6614	0.6614	0.6640	0.6833
Al-Al_2O_3	1	0.7690	0.6623	0.6540	0.6556	0.6871	0.7860	0.6871	0.6556	0.6540	0.6623	0.7690
	1.25	0.8080	0.6650	0.6552	0.6564	0.6882	0.7860	0.6882	0.6564	0.6552	0.6650	0.8080
	1.5	0.8618	0.6679	0.6564	0.6572	0.6892	0.7860	0.6892	0.6572	0.6564	0.6679	0.8618
	1.75	0.9404	0.6709	0.6576	0.6580	0.6903	0.7860	0.6903	0.6580	0.6576	0.6709	0.9404
	2	1.0642	0.6740	0.6589	0.6589	0.6914	0.7860	0.6914	0.6589	0.6589	0.6740	1.0642
Al-ZrO_2	1	0.5609	0.5603	0.5671	0.5654	0.5549	0.8146	0.5549	0.5654	0.5671	0.5603	0.5609
	1.25	0.5640	0.5590	0.5658	0.5646	0.5549	0.8146	0.5549	0.5646	0.5658	0.5590	0.5640
	1.5	0.5675	0.5578	0.5646	0.5639	0.5549	0.8146	0.5549	0.5639	0.5646	0.5578	0.5675
	1.75	0.5712	0.5569	0.5635	0.5632	0.5549	0.8146	0.5549	0.5632	0.5635	0.5569	0.5712
	2	0.5751	0.5562	0.5626	0.5626	0.5549	0.8146	0.5549	0.5626	0.5626	0.5562	0.5751

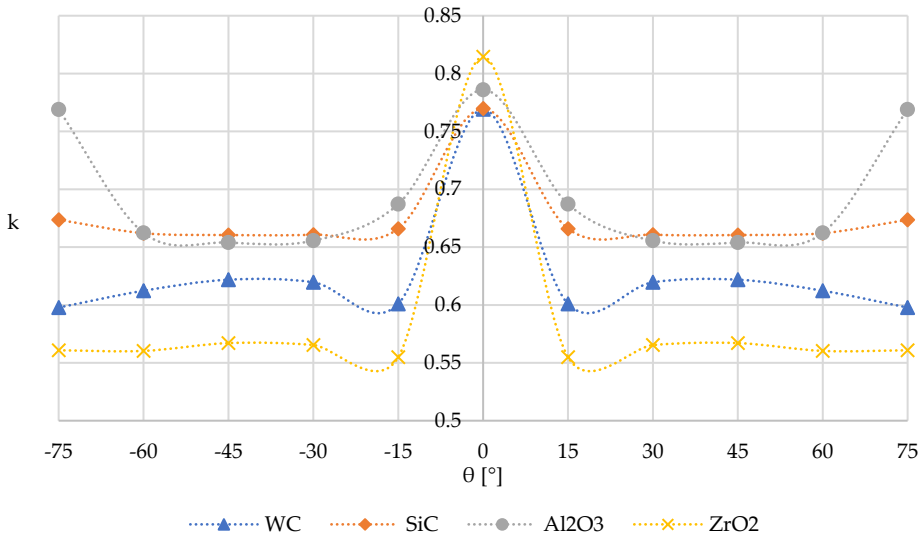

Figure 13. Shear correction factor for different FGM auxetic beams with a/h = 10 and unit cells with $\eta 1 = 1$ and $\eta 3 = 0.01$.

3.2.4. Non-Dimensional Maximum Beams' Static Deflection—Influence of the Cell's Aspect Ratios $\eta 1$, $\eta 3$ and the Angle θ

This case studies the influence of the unit cell aspect ratios $\eta 1$ and $\eta 3$ and the angle θ in the non-dimensional maximum static deflection of the honeycomb auxetic beam. The FGM selected for this purpose was the Al-WC, and the length-to-thickness ratio of the beam was set to 20.

The results achieved are presented in Table 7 in a non-dimensional form using the multiplier $\hat{w} = \frac{E_m \cdot w \cdot h^3}{10^3 p_z a^4}$, where E_m is the Young's modulus of the metallic phase, h is the beam thickness, a stands for the beam length, and p_z the uniformly distributed load.

Table 7. Non-dimensional maximum static deflection of Al-WC auxetic beam, with a/h = 20.

		θ [°]										
η3	**η1**	**−75**	**−60**	**−45**	**−30**	**−15**	**0**	**15**	**30**	**45**	**60**	**75**
0.01	1	0.3670	2.5108	7.5948	15.9016	27.4976	57.3780	46.6920	47.6597	44.1459	34.7041	20.5078
	1.25	0.3314	2.2280	6.6459	13.6570	22.9680	45.9036	34.9555	31.8357	23.8918	12.1811	2.4977
	1.5	0.3027	2.0047	5.9117	11.9733	19.7260	38.2539	27.9468	23.9235	16.4095	7.4209	1.3481
	1.75	0.2791	1.8239	5.3267	10.6637	17.2908	32.7899	23.2880	19.1759	12.5143	5.3528	0.9314
	2	0.2593	1.6744	4.8497	9.6158	15.3946	28.6919	19.9669	16.0107	10.1252	4.1963	0.7161
0.02	1	0.0532	0.3459	1.0229	2.1515	3.8840	7.1744	6.5952	6.4485	5.9457	4.7802	2.9684
	1.25	0.0482	0.3085	0.8986	1.8524	3.2464	5.7401	4.9407	4.3180	3.2305	1.6866	0.3625
	1.5	0.0441	0.2789	0.8023	1.6278	2.7900	4.7839	3.9527	3.2524	2.2270	1.0323	0.1960
	1.75	0.0407	0.2548	0.7255	1.4531	2.4472	4.1009	3.2959	2.6129	1.7043	0.7478	0.1356
	2	0.0379	0.2349	0.6627	1.3131	2.1802	3.5887	2.8277	2.1863	1.3835	0.5884	0.1044
0.03	1	0.0173	0.1116	0.3267	0.6883	1.2516	2.1268	2.1252	2.0629	1.8990	1.5416	0.9628
	1.25	0.0157	0.0997	0.2876	0.5933	1.0462	1.7018	1.5922	1.3829	1.0338	0.5448	0.1175
	1.5	0.0143	0.0902	0.2572	0.5219	0.8992	1.4185	1.2739	1.0428	0.7139	0.3339	0.0635
	1.75	0.0132	0.0825	0.2329	0.4663	0.7887	1.2162	1.0623	0.8385	0.5472	0.2421	0.0440
	2	0.0123	0.0761	0.2131	0.4218	0.7027	1.0644	0.9114	0.7022	0.4448	0.1906	0.0338
0.04	1	0.0078	0.0502	0.1466	0.3086	0.5572	0.8979	0.9462	0.9250	0.8521	0.6933	0.4327
	1.25	0.0071	0.0448	0.1291	0.2661	0.4658	0.7186	0.7089	0.6203	0.4641	0.2450	0.0528
	1.5	0.0065	0.0406	0.1155	0.2341	0.4003	0.5991	0.5671	0.4678	0.3207	0.1501	0.0286
	1.75	0.0060	0.0371	0.1047	0.2092	0.3511	0.5137	0.4729	0.3762	0.2458	0.1089	0.0198
	2	0.0056	0.0342	0.0958	0.1893	0.3128	0.4497	0.4058	0.3151	0.1999	0.0857	0.0152
0.05	1	0.0042	0.0270	0.0788	0.1655	0.2958	0.4601	0.5023	0.4962	0.4578	0.3726	0.2332
	1.25	0.0038	0.0241	0.0694	0.1427	0.2473	0.3683	0.3763	0.3327	0.2494	0.1316	0.0285
	1.5	0.0035	0.0218	0.0621	0.1256	0.2125	0.3071	0.3011	0.2509	0.1723	0.0807	0.0154
	1.75	0.0032	0.0199	0.0562	0.1122	0.1864	0.2634	0.2511	0.2018	0.1321	0.0585	0.0107
	2	0.0031	0.0184	0.0514	0.1015	0.1661	0.2306	0.2154	0.1690	0.1074	0.0460	0.0083

From the results in Table 7, we conclude that, for the present case, the non-dimensional maximum static deflection decreases when $\eta 1$ increases (in absolute value). This is true for any angle θ and for any aspect ratio $\eta 3$. We can also conclude that, for a specific pair of aspect ratios $\eta 1$ and $\eta 3$, this deflection gradually increases up to a maximum value correspondent to $\theta = 0^\circ$ and starts decreasing after that, with minor values obtained for the angles $\theta = -75^\circ$ and $\theta = 75^\circ$. For these latter cases, the cells present a "flattened" configuration.

From the table, it is also visible that, as expected, the non-dimensional maximum static deflection decreases as the ratio $\eta 3$ increases.

Figures 14 and 15 illustrate the non-dimensional maximum static deflection for the discrete values in the sets of geometrical parameters θ and $\eta 1$ and for the two limit values of $\eta 3$. These values correspond to the thinner ($\eta 3 = 0.01$) and thicker ($\eta 3 = 0.05$) unit cell configurations considered in the present study.

As one observes, the evolution of the non-dimensional maximum deflection presents a stepwise profile function of the angle θ. For each specific angle, when $\eta 1$ increases, i.e., the unit cell tends to a flattened configuration, the deflection always decreases.

Regarding the influence of the unit cell thickness, it is clear from both figures that the beam made of the auxetic material with thicker cell walls presents, as expected, significant reductions in the maximum deflection.

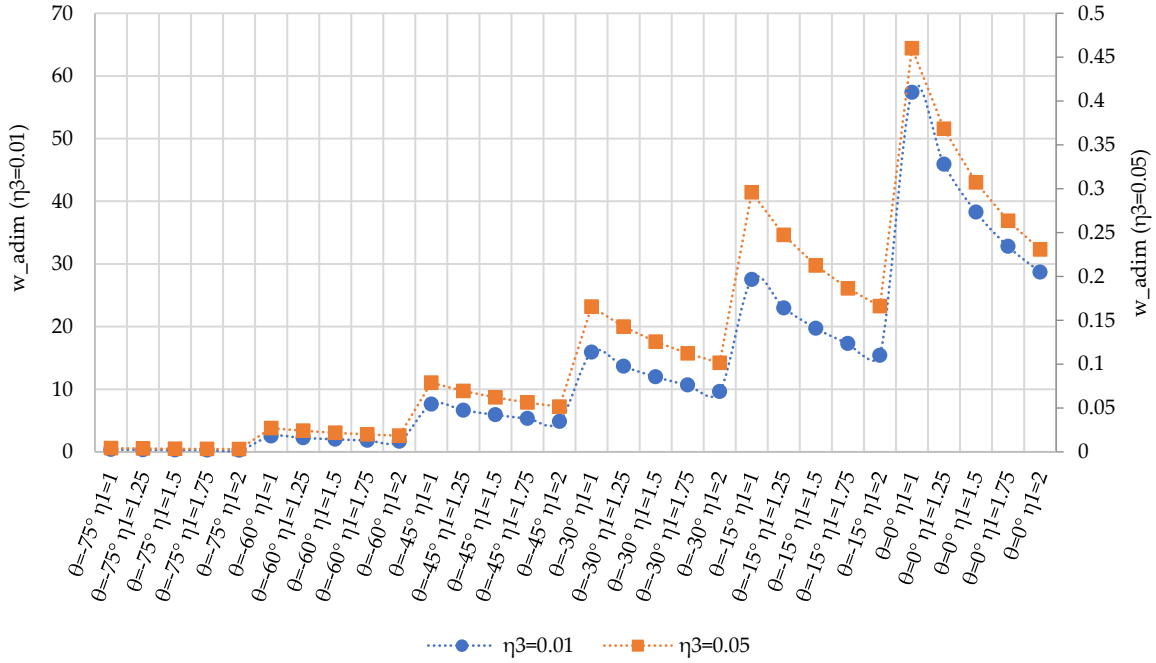

Figure 14. Non-dimensional maximum static deflection of Al-WC FGM honeycomb auxetic beams with a/h = 20 within the range of angles $\theta = -75°$ to $\theta = 0°$

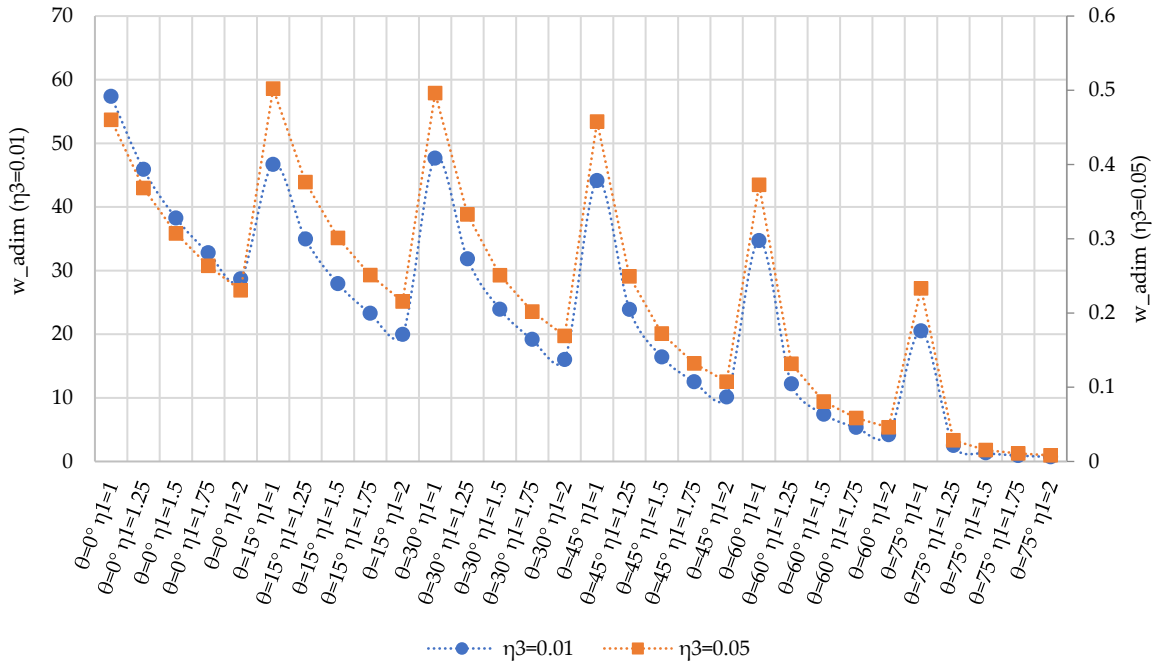

Figure 15. Non-dimensional maximum static deflection of Al-WC FGM auxetic beams with a/h = 20, within the range of angles $\theta = 0°$ to $\theta = 75°$

3.2.5. Non-Dimensional Maximum Beams' Static Deflection—Influence of Constituent Materials

The influence of the constituent materials of the honeycomb auxetic FGM, more specifically the ceramic materials used (Table 3), is analyzed in the present case. The beams studied have a length-to-thickness ratio of 20, and the re-entrant hexagonal cells are characterized by $\eta 3 = 0.05$. The non-dimensional maximum deflections, given as $\hat{w} = \frac{E_m \cdot w \cdot h^3}{10^3 p_z a^4}$, are presented in Table 8.

Table 8. Non-dimensional maximum static deflection of all auxetic beams with a/h = 20 as a function of θ, $\eta 1$ and $\eta 3$.

		θ [°]										
Material	**η1**	**−75**	**−60**	**−45**	**−30**	**−15**	**0**	**15**	**30**	**45**	**60**	**75**
Al-WC	1	0.0042	0.0270	0.0788	0.1655	0.2958	0.4601	0.5023	0.4962	0.4578	0.3726	0.2332
	1.25	0.0038	0.0241	0.0694	0.1427	0.2473	0.3683	0.3763	0.3327	0.2494	0.1316	0.0285
	1.5	0.0035	0.0218	0.0621	0.1256	0.2125	0.3071	0.3011	0.2509	0.1723	0.0807	0.0154
	1.75	0.0032	0.0199	0.0562	0.1122	0.1864	0.2634	0.2511	0.2018	0.1321	0.0585	0.0107
	2	0.0031	0.0184	0.0514	0.1015	0.1661	0.2306	0.2154	0.1690	0.1074	0.0460	0.0083
Al-SiC	1	0.0050	0.0418	0.1254	0.2610	0.4957	0.5115	0.8418	0.7819	0.7287	0.5754	0.2779
	1.25	0.0048	0.0373	0.1103	0.2241	0.4192	0.4095	0.6380	0.5223	0.3940	0.2029	0.0353
	1.5	0.0043	0.0337	0.0976	0.1966	0.3651	0.3414	0.5172	0.3925	0.2705	0.1244	0.0196
	1.75	0.0042	0.0311	0.0880	0.1751	0.3252	0.2928	0.4379	0.3147	0.2065	0.0905	0.0139
	2	0.0041	0.0286	0.0801	0.1592	0.2948	0.2564	0.3824	0.2630	0.1671	0.0718	0.0111
Al-Al_2O_3	1	0.0052	0.0340	0.0615	0.1622	0.1608	0.5554	0.2730	0.4859	0.3571	0.4703	0.2854
	1.25	0.0096	0.0317	0.0652	0.1490	0.2009	0.4446	0.3058	0.3473	0.2343	0.1727	0.0370
	1.5	0.0048	0.0297	0.0648	0.1375	0.1999	0.3707	0.2832	0.2746	0.1797	0.1097	0.0205
	1.75	0.0043	0.0286	0.0628	0.1275	0.1895	0.3180	0.2552	0.2374	0.1473	0.0837	0.0115
	2	0.0196	0.3347	0.0601	0.1187	0.1771	0.2784	0.2297	0.1977	0.1255	0.8545	0.0160
Al-ZrO_2	1	0.0068	0.0436	0.1271	0.2672	0.4787	0.7456	0.8128	0.8009	0.7388	0.6021	0.3777
	1.25	0.0062	0.0390	0.1120	0.2304	0.4001	0.5969	0.6090	0.5371	0.4025	0.2128	0.0462
	1.5	0.0057	0.0353	0.1002	0.2028	0.3439	0.4977	0.4873	0.4052	0.2782	0.1304	0.0250
	1.75	0.0053	0.0323	0.0908	0.1813	0.3017	0.4269	0.4063	0.3259	0.2133	0.0946	0.0174
	2	0.0049	0.0298	0.0831	0.1640	0.2688	0.3738	0.3486	0.2730	0.1735	0.0745	0.0134

In addition to the relative stiffness character of the beams built with the different materials, the results achieved identify two main trend profiles, one presented by the auxetic FGM Al-WC and Al-ZrO_2 and the other presented by the auxetic Al-SiC and Al-Al_2O_3. The first two materials confer upon the beams a non-dimensional maximum deflection that progressively increases from the -75° angle to the 15° angle and then starts decreasing. The second material, where the constituent materials of the beam present very different Poisson ratios, provides the beam's maximum non-dimensional deflection profiles as an oscillating trend that is more visible in the Al-Al_2O_3 case.

4. Conclusions

The present work's main goal was to characterize the influence that material and geometrical features of re-entrant hexagonal honeycomb auxetic structures have on the shear correction factor required by the first-order shear deformation factor and on the maximum static deflection of beams made solely of such materials. For this purpose, a set of case studies were considered. Firstly, one has characterized the Poisson ratios and the bending and transverse shear stiffness coefficients for different auxetic FGM beams. Following this, two other case studies focused on the shear correction factor were conducted to assess how this factor is influenced by the unit cell aspect ratios $\eta 1$ and $\eta 3$, the angle θ and by the material properties of the structure. The two final case studies were meant to investigate the influence of those parameters on the beams' maximum static deflection.

From the results achieved, it is possible to conclude that the mixture of constituent materials with more differentiated Poisson ratios, namely the Al-SiC and Al-Al_2O_3 FGM, when compared with the Al-WC and Al-ZrO_2 FGM, which have closer Poisson ratios, significantly influence the different stiffness coefficients of the resulting structural composite. The resulting Poisson's ratios of the honeycomb auxetic material also demonstrate to be very influenced by this. These conclusions are aligned with (Evans, 1991) [1], namely regarding the importance that the Poisson ratio may have on a structure's behavior improvement, and thus, the need to address this aspect.

Concerning the shear correction factor, it was found that the Al-WC and Al-ZrO_2 FGM auxetic materials share a similar evolution profile, while the Al-Al_2O_3 and Al-SiC FGM honeycomb auxetic materials present another trend. This is attributed to the influence of the greater or lesser similarity of the constituent materials' Poisson ratios. Regarding the geometric parameters, the angle θ of the unit cell has a great influence on the shear correction factor, as the unit cell aspect ratio $\eta 3$ does. The influence of the aspect ratio $\eta 1$, although visible, is minor when compared with $\eta 3$.

Concerning the beams' maximum transverse deflection, it was again possible to identify two trends. When the FGM constituent materials possess closer Poisson ratios, the beams' non-dimensional maximum deflection increases from the angle $\theta = -75^\circ$ to the angle $\theta = 15^\circ$ and then starts decreasing. When the Poisson ratios of the ceramic materials are lower than that of the aluminum, the beam's maximum non-dimensional deflection profiles present an oscillating trend regarding the evolution along the different angles studied. Regarding the geometrical parameters, the influence of the aspect ratio $\eta 1$ on the non-dimensional maximum deflection is more effective for angles between $\theta = -30^\circ$ and $\theta = 60^\circ$. Note that, when considering the evolution of this quantity as a function of the angle, for positive angles and when $\eta 1 = 1$, the decreasing trend is slighter in comparison with other $\eta 1$ values. The relation between the thickness of the cell and the length of the inclined segments ($\eta 3$) shows a direct influence on the maximum deflection.

Considering the relevance of these structural materials, further studies on this topic are foreseen to exploit other potential benefits that their use or integration within other structures may bring.

Author Contributions: Conceptualization, M.A.R.L. and J.I.B.; methodology, M.A.R.L. and J.I.B.; software, M.A.R.L. and J.I.B.; validation, M.A.R.L. and J.I.B.; formal analysis, M.A.R.L. and J.I.B.; investigation, M.A.R.L. and J.I.B.; data curation, M.A.R.L. and J.I.B.; writing—original draft preparation, M.A.R.L. and J.I.B.; writing—review and editing, M.A.R.L. and J.I.B.; visualization, M.A.R.L. and J.I.B. All authors have read and agreed to the published version of the manuscript.

Funding: This research received no external funding.

Data Availability Statement: The original contributions presented in the study are included in the article, further inquiries can be directed to the corresponding author.

Acknowledgments: The authors would like to acknowledge the support provided by the Fundação para a Ciência e a Tecnologia (FCT) and IDMEC for its financial support via the project LAETA Base Funding (DOI: 10.54499/UIDB/50022/2020).

Conflicts of Interest: The authors declare no conflicts of interest.

References

1. Evans, K.E. Auxetic polymers: A new range of materials. *Endeavour* **1991**, *15*, 170–174. [CrossRef]
2. Almgren, R.F. An isotropic three-dimensional structure with Poisson's ratio = −1. *J. Elast.* **1985**, *15*, 427–430.
3. Lakes, R. Foam Structures with a Negative Poisson's Ratio. *Science* **1987**, *235*, 1038–1040. [CrossRef] [PubMed]
4. Wojciechowski, K. Two-Dimensional Isotropic System with a Negative Poisson Ratio. *Phys. Lett. A* **1989**, *137*, 60–64. [CrossRef]
5. Milton, G.W. Composite Materials with Poisson Ratios Close to −1. *J. Phys. Chem. Solids* **1992**, *40*, 1105–1137. [CrossRef]
6. Koizumi, M. FGM activities in Japan. *Compos. Part B Eng.* **1997**, *28*, 1–4. [CrossRef]
7. Zhang, Q.; Yang, X.; Li, P.; Huang, G.; Feng, S.; Shen, C.; Han, B.; Zhang, X.; Jin, F.; Xu, F.; et al. Bioinspired engineering of honeycomb structure—Using nature to inspire human innovation. *Prog. Mater. Sci.* **2015**, *74*, 332–400. [CrossRef]
8. Sahu, S.K.; Sreekanth, P.S.R.; Reddy, S.V.K. A Brief Review on Advanced Sandwich Structures with Customized Design Core and Composite Face Sheet. *Polymers* **2022**, *14*, 4267. [CrossRef]
9. Evans, K.E.; Alderson, A. Auxetic Materials: Functional Materials and Structures from Lateral Thinking! *Adv. Mater.* **2000**, *12*, 617–628. [CrossRef]
10. Prawoto, Y. Seeing auxetic materials from the mechanics point of view: A structural review on the negative Poisson's ratio. *Comput. Mater. Sci.* **2012**, *58*, 140–153. [CrossRef]
11. Liu, Y.; Zhao, C.; Xu, C.; Ren, J.; Zhong, J. Auxetic meta-materials and their engineering applications: A review. *Eng. Res. Express* **2023**, *5*, 042003. [CrossRef]
12. Masters, I.; Evans, K. Models for the elastic deformation of honeycombs. *Compos. Struct.* **1996**, *35*, 403–422. [CrossRef]

13. Strek, T.; Jopek, H.; Nienartowicz, M. Dynamic response of sandwich panels with auxetic cores. *Phys. Status Solidi B* **2015**, *252*, 1540–1550. [CrossRef]
14. Scarpa, F.; Tomlin, P.J. On the transverse shear modulus of negative Poisson's ratio honeycomb structures. *Fatigue Fract. Eng. Mater. Struct.* **2000**, *23*, 717–720. [CrossRef]
15. Gao, Q.; Ding, Z.; Liao, W.-H. Effective elastic properties of irregular auxetic structures. *Compos. Struct.* **2022**, *287*, 115269. [CrossRef]
16. Ghalehney, S.M.; Sadeghi, M.H.; Gharehbaghi, H. Mechanical Properties of 2D Re-Entrant Gradient Structures Produced by Additive Manufacturing. *Iran. J. Sci. Technol. Trans. Mech. Eng.* **2024**, *48*, 1395–1404. [CrossRef]
17. Zhang, X.; Deng, Q.; Song, X.; Li, X. Elastic Properties and Energy Absorption of Irregular Auxetic Cellular Structure. *J. Mater. Eng. Perform.* **2024**. [CrossRef]
18. Valle, R.; Pincheira, G.; Tuninetti, V. Design of an auxetic cellular structure with different elastic properties in its three orthogonal directions. *Proc. Inst. Mech. Eng. Part L J. Mater. Des. Appl.* **2021**, *235*, 1341–1350. [CrossRef]
19. Bhullar, S.K.; Lekesiz, H.; Karaca, A.A.; Cho, Y.; Willerth, S.M.; Jun, M.B.G. Characterizing the Mechanical Performance of a Bare-Metal Stent with an Auxetic Cell Geometry. *Appl. Sci.* **2022**, *12*, 910. [CrossRef]
20. Luo, Y.; Dai, F.; Shen, J.; Wang, A.; Jiang, X.; Li, Y. Negative Poisson's Ratio Lattice Structure with Chiral and Re-Entrant Properties. *Appl. Sci.* **2023**, *13*, 13097. [CrossRef]
21. Qing-Tian, D.; Zhi-Chun, Y. Wave Propagation in Sandwich Panel with Auxetic Core. *J. Solid Mech.* **2010**, *2*, 393–402.
22. Rad, M.S.; Prawoto, Y.; Ahmad, Z. Analytical solution and finite element approach to the 3D re-entrant structures of auxetic materials. *Mech. Mater.* **2014**, *74*, 76–87. [CrossRef]
23. Chen, X.; Feng, Z. Dynamic behaviour of a thin laminated plate embedded with auxetic layers subject to in-plane excitation. *Mech. Res. Commun.* **2017**, *85*, 45–52. [CrossRef]
24. Duncan, O.; Shepherd, T.; Moroney, C.; Foster, L.; Venkatraman, P.D.; Winwood, K.; Allen, T.; Alderson, A. Review of Auxetic Materials for Sports Applications: Expanding Options in Comfort and Protection. *Appl. Sci.* **2018**, *8*, 941. [CrossRef]
25. Duc, N.D.; Seung-Eock, K.; Tuan, N.D.; Tran, P.; Khoa, N.D. New approach to study nonlinear dynamic response and vibration of sandwich composite cylindrical panels with auxetic honeycomb core layer. *Aerosp. Sci. Technol.* **2017**, *70*, 396–404. [CrossRef]
26. Nguyen, D.D.; Pham, C.H. Nonlinear dynamic response and vibration of sandwich composite plates with negative Poisson's ratio in auxetic honeycombs. *J. Sandw. Struct. Mater.* **2018**, *20*, 692–717. [CrossRef]
27. Zhu, X.; Zhang, J.; Zhang, W.; Chen, J. Vibration frequencies and energies of an auxetic honeycomb sandwich plate. *Mech. Adv. Mater. Struct.* **2019**, *26*, 1951–1957. [CrossRef]
28. Tran, T.T.; Pham, Q.H.; Nguyen-Thoi, T.; Tran, T.-V. Dynamic Analysis of Sandwich Auxetic Honeycomb Plates Subjected to Moving Oscillator Load on Elastic Foundation. *Adv. Mater. Sci. Eng.* **2020**, *2020*, 1–16. [CrossRef]
29. Nasim, M.S.; Yaghootian, A.; Mosalmani, R. Energy absorption of the additively manufactured novel re-entrant auxetic structure in comparison with honeycomb structure: Experimental and numerical analysis. *J. Braz. Soc. Mech. Sci. Eng.* **2023**, *45*, 275. [CrossRef]
30. Birman, V.; Byrd, L.W. Modeling and Analysis of Functionally Graded Materials and Structures. *Appl. Mech. Rev.* **2007**, *60*, 195–216. [CrossRef]
31. Zhang, J.-H.; Dong, B.-J.; He, B.; Sun, Y. Free Vibrations and Impact Resistance of a Functionally Graded Honeycomb Sandwich Plate. *Shock. Vib.* **2021**, *2021*, 1–15. [CrossRef]
32. Li, F.; Yuan, W.; Zhang, C. Free vibration and sound insulation of functionally graded honeycomb sandwich plates. *J. Sandw. Struct. Mater.* **2022**, *24*, 565–600. [CrossRef]
33. Mindlin, R.D. Influence of Rotatory Inertia and Shear on Flexural Motions of Isotropic, Elastic Plates. *J. Appl. Mech.* **1951**, *18*, 31–38. [CrossRef]
34. Reissner, E. The Effect of Transverse Shear Deformation on the Bending of Elastic Plates. *J. Appl. Mech.* **1945**, *12*, A69–A77. [CrossRef]
35. Carvalho, A.; Silva, T.; Loja, M.A.R.; Damásio, F.R. Assessing the influence of material and geometrical uncertainty on the mechanical behavior of functionally graded material plates. *Mech. Adv. Mater. Struct.* **2017**, *24*, 417–426. [CrossRef]
36. Rosa, R.D.S.B.; Loja, M.A.R.; de Carvalho, A.C.J.V.N. Toward Variability Characterization and Statistic Models' Constitution for the Prediction of Exponentially Graded Plates' Static Response. *J. Compos. Sci.* **2018**, *2*, 59. [CrossRef]
37. Reddy, J.N. Analysis of functionally graded plates. *Int. J. Numer. Methods Eng.* **2000**, *47*, 663–684. [CrossRef]
38. Reddy, J.N. *Mechanics of Laminated Composite Plates and Shells*; CRC Press: Boca Raton, FL, USA, 2003.
39. Whitney, J.M. Shear Correction Factors for Orthotropic Laminates Under Static Load. *J. Appl. Mech.* **1973**, *40*, 302–304. [CrossRef]
40. Mota, A.F.; Loja, M.A.R.; Barbosa, J.I.; Rodrigues, J.A. Porous functionally graded plates: An assessment of the influence of shear correction factor on static behavior. *Math. Comput. Appl.* **2020**, *25*, 25. [CrossRef]
41. Mota, A.F.; Loja, M.A.R. A study on porous nanocomposite graded plates using equivalent single layer and layerwise models. *Mech. Adv. Mater. Struct.* **2023**, *30*, 4155–4177. [CrossRef]
42. Vlachoutsis, S. Shear correction factors for plates and shells. *Int. J. Numer. Methods Eng.* **1992**, *33*, 1537–1552. [CrossRef]
43. Zienkiewicz, O.C.; Taylor, R.L. *The Finite Element Method for Solid and Structural Mechanics*, 6th ed.; Elsevier: Amsterdam, The Netherlands, 2014.

44. Loja, M.; Barbosa, J.; Scares, C. Buckling behaviour of laminated beam structures using a higher-order discrete model. *Compos. Struct.* **1997**, *38*, 119–131. [CrossRef]
45. Sengupta, D. Stress analysis of flat plates with shear using explicit stiffness matrix. *Int. J. Numer. Methods Eng.* **1991**, *32*, 1389–1409. [CrossRef]
46. Rao, G.; Venkataramana, J.; Raju, I. A high precision triangular plate bending element for the analysis of thick plates. *Nucl. Eng. Des.* **1974**, *30*, 408–412. [CrossRef]
47. Salerno, V.L.; Goldberg, M.A. Effect of Shear Deformations on the Bending of Rectangular Plates. *J. Appl. Mech.* **1960**, *27*, 54–58. [CrossRef]
48. Nguyen, T.-K.; Sab, K.; Bonnet, G. First-order shear deformation plate models for functionally graded materials. *Compos. Struct.* **2008**, *83*, 25–36. [CrossRef]